Frustration-induced two-dimensional quantum disordered phase in piperazinium hexachlorodicuprate

M. B. Stone,[1] I. Zaliznyak,[1,3] Daniel H. Reich,[1] and C. Broholm[1,2]

[1]*Department of Physics and Astronomy, The Johns Hopkins University, Baltimore, Maryland 21218*
[2]*National Institute of Standards and Technology, Gaithersburg, Maryland 20899*
[3]*Department of Physics, Brookhaven National Laboratory, Upton, New York 11973-5000*

Piperazinium hexachlorodicuprate is shown to be a frustrated quasi-two-dimensional quantum Heisenberg antiferromagnet with a gapped spectrum. Zero-field inelastic neutron scattering and susceptibility and specific-heat measurements as a function of applied magnetic field are presented. At $T = 1.5$ K, the magnetic excitation spectrum is dominated by a single propagating mode with a gap, $\Delta = 1$ meV, and bandwidth of ≈ 1.8 meV in the $(h0l)$ plane. The mode has no dispersion along the $b*$ direction indicating that neighboring **a**-**c** planes of the triclinic structure are magnetically decoupled. The heat capacity shows a reduction of the gap as a function of applied magnetic field in agreement with a singlet-triplet excitation spectrum. A field-induced ordered phase is observed in heat capacity and magnetic susceptibility measurements for magnetic fields greater than $H_{c1} \approx 7.5$ T. Analysis of the neutron-scattering data reveals the important exchange interactions and indicates that some of these are highly frustrated.

PACS number(s): 75.10.Jm, 75.40.Gb, 75.50.Ee

I. INTRODUCTION

Among physical systems that display collective macroscopic quantum phenomena, interacting spin systems are perhaps the most experimentally informative. Many qualitatively different model systems are available, and there are numerous experimental tools providing access to spatial and temporal correlations on microscopic, mesoscopic, and macroscopic scales. Owing to their relative simplicity, much attention has been devoted to one-dimensional systems, such as the spin $S = 1$ Haldane chain,[1] the even-leg $S = 1/2$ spin ladders,[2–4] and dimerized (alternating bond) $S = 1/2$ chains.[5–7] However, it has long been a quest for theorists and experimentalists alike to find analogous cooperative singlet ground-state magnetism in higher dimensions.

For the two-dimensional $S = 1/2$ quantum Heisenberg antiferromagnet (2D QHAFM), a nontrivial quantum-disordered spin-gap phase with a singlet ground state in the vicinity of a quantum-critical point has been studied extensively by theorists in relation to the magnetic properties of layered cuprate superconductors.[8,9] Several models were suggested to fall into this quantum-disordered phase, ranging from simple quantum dimer models,[10] and a valence bond crystal favored by frustration on the 2D square lattice,[11,12] to the quantum *kagomé* antiferromagnet[13–15] and the long-sought spin-liquid resonating valence bond (RVB) state.[16,17] While there are numerous materials which, like the layered cuprates, fall into the renormalized-classical region of the phase diagram of the 2D QHAFM, realizations of quantum disordered 2D spin systems close to the quantum critical point are scarce.

There are higher dimensional coupled spin dimer systems such as the three-dimensional dimer networks $Cs_3Cr_2Br_9$,[18] $KCuCl_3$,[19,20] and $TlCuCl_3$,[21,22] and the quasi-2D material $BaCuSi_2O_6$.[23] However, as with strongly dimerized linear chains such as $Cu(NO_3)_2 \cdot 2.5D_2O$,[5] correlations in these systems are dominated by isolated spin pairs. For different reasons, this is also the case in the two-dimensional frustrated spin system $SrCu_2(BO_3)_2$.[24] In that material, triplet excitations are localized because of the frustrating symmetry of the interactions.[25] Here we report a frustration-induced spin-singlet phase with a gapped spectrum in the metalo-organic compound piperazinium hexachlorodicuprate (PHCC). The important distinction from other $D > 1$ singlet systems is that there are uniform extensive paths of interaction spanning the quasi-2D plane and the strongly correlated spin cluster in PHCC involves several spin pairs. Even so there is a spin gap in the excitation spectrum, and no magnetic phase transition in the absence of a magnetic field.

These results were obtained through an extensive characterization of PHCC using magnetic susceptibility, specific heat, and inelastic neutron-scattering measurements. Our findings correct previous reports that suggest that PHCC is an alternating spin chain system.[26–28] In agreement with previous thermodynamic data, we find a triplet mode with a spin gap $\Delta = 1$ meV, and a bandwidth of 1.8 meV. However, rather than the dispersion being confined to the putative chain direction **c**, we observe dispersion throughout the **a**-**c** plane. In addition, our analysis of the wave-vector-dependent scattering intensity shows that no fewer than five spin pairs are strongly correlated. Two of these provide *positive* contributions to the ground-state energy, indicating the presence of frustration. We also present evidence for a field-induced magnetic phase transition that provides an interesting example of quantum critical behavior in a frustrated quasi-two-dimensional spin system.

II. PIPERAZINIUM HEXACHLORODICUPRATE

Piperazinium hexachlorodicuprate (PHCC), $(C_4H_{12}N_2)Cu_2Cl_6$, has a triclinic crystal structure with space group $P\bar{1}$, and room-temperature lattice constants a
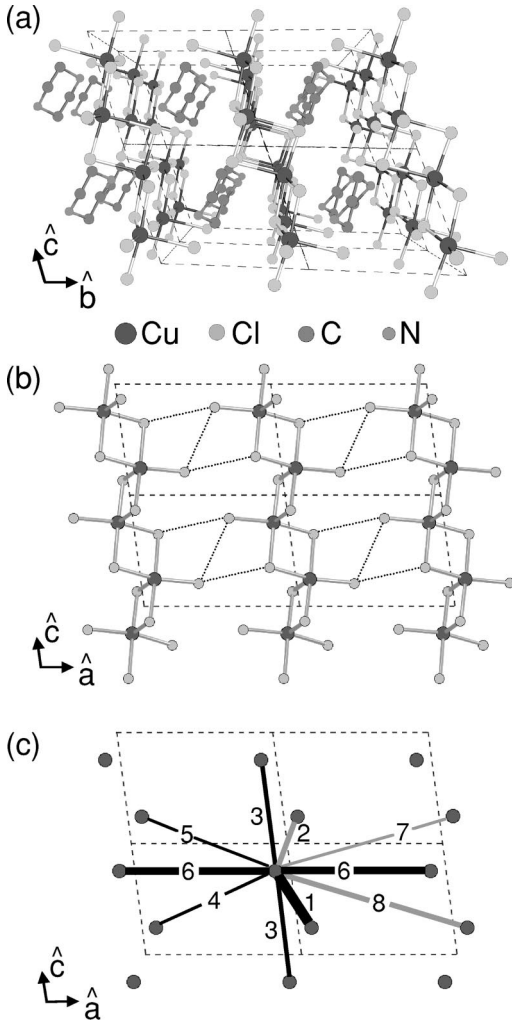
(a)

● Cu ● Cl ● C ● N

(b)

(c)

FIG. 1. Crystal structure of piperazinium hexachlorodicuprate (PHCC), $(C_4H_{12}N_2)(Cu_2Cl_6)$. (a) View along the **a** axis showing well-separated Cu-Cl planes. (b) A single Cu-Cl plane viewed along the **b** axis, showing four unit cells. The dotted lines indicate possible halide-halide contacts (see text). (c) Cu-Cu interactions that contribute to the magnetic Hamiltonian (see Table I). The line thickness is proportional to $|J_d\langle S_0 \cdot S_d \rangle|$ for each bond. The gray lines indicate frustrated bonds.

$=7.984(4)$ Å, $b=7.054(4)$ Å, $c=6.104(3)$ Å, and $\alpha = 111.23(8)°$, $\beta=99.95(9)°$, and $\gamma=81.26(7)°$. (We use the nomenclature of Ref. 26.) The lattice parameters at temperature $T=1.5$ K were found to be $a=7.82(2)$, $b=6.7(3)$, and $c=5.8(2)$ Å.

The crystal structure of PHCC is depicted in Fig. 1. Figure 1(a) is a perspective drawing of the crystal structure as viewed along the **a** axis. Copper-chlorine layers in the **a-c** plane are clearly visible. These are well separated from one another by the piperazinium dication rings. By rotating the structure in Fig. 1(a) about the **c** axis, one obtains the view shown in Fig. 1(b), which depicts a single copper-chlorine plane. The Cu^{2+} ions have a distorted 4+1 coordination with their neighboring chlorine atoms. The four short Cu-Cl bonds, with an average bond length of 2.30 Å, are approximately coplanar, with the long 2.62 Å Cu-Cl bond nearly

TABLE I. Fractional coordinates (from Ref. 20), bond lengths, and corresponding values of $J_d\langle S_0 \cdot S_d \rangle$ (in meV) for the fits of the PHCC inelastic neutron-scattering data including six and eight Cu-Cu bonds. Bond numbers correspond to those depicted in Fig. 1(c).

Bond number	x/a	y/b	z/c	$|d|$ (Å)	6 bonds $J_d\langle S_0 \cdot S_d \rangle$	8 bonds $J_d\langle S_0 \cdot S_d \rangle$
1	−0.19	0.12	0.51	3.450	−1.3(3)	−1.4(3)
2	0.19	−0.12	0.49	3.442	0.7(3)	0.6(3)
3	0	0	1	6.104	−0.3(1)	−0.4(1)
4	0.81	0.12	0.51	6.730	0.1(3)	−0.2(3)
5	0.81	0.12	−0.49	7.879	−0.0(3)	−0.1(3)
6	1	0	0	7.984	−0.92(5)	−0.95(5)
7	1.19	−0.12	0.49	9.439		0.1(2)
8	−1.19	0.12	0.51	10.296		0.6(2)

perpendicular to this plane. With this coordination, the Cu^{2+} spin density lies predominantly in the four-bond plane, and therefore Cu-Cl-Cu superexchange interactions that involve only the short Cu-Cl bonds should be stronger than those involving the long bonds. On this basis, the magnetic Cu-Cu interaction indicated by bond 1 in Fig. 1(c) was predicted to be stronger than bond 2,[27] leading to the alternating chain model.[26–28] However, our neutron-scattering results show that while the spins interacting through bond 1 are indeed the most strongly correlated, Cu-Cu couplings not previously considered, such as those due to the halide-halide contacts shown as dotted lines in Fig. 1(b), result in dispersion along the **a** direction that is stronger than that along **c**. As we will show, PHCC contains a two-dimensional network of magnetic interactions in the **a-c** plane. The Cu-Cu interactions that we will consider in our analysis are numbered 1–8 in Fig. 1(c). Our results pertaining to these bonds are listed in Table I.

III. EXPERIMENTAL TECHNIQUES

Powder samples of PHCC were prepared by rapid cooling from 50 to 0 °C of 38% hydrochloric acid solutions containing piperazinium dihydrochloride and copper(II) chloride in a 1:4 molar ratio.[26] Single crystals were grown by slowly reducing the temperature of similar saturated solutions from 50 to 18 °C over 75 h. Seed crystals obtained in this manner were suspended in saturated solutions and grown further. The crystals typically grow as dark red tablets with (100) faces providing the largest facets. Deuterated single crystals for the inelastic neutron-scattering measurements were produced in this manner from commercially available piperazinium (d_8) dihydrochloride and anhydrous copper chloride(II), using 35% DCl in D_2O as the solvent. The crystals were 89(1)% deuterated, as determined by neutron activation analysis.

Low-field dc magnetic susceptibility measurements were performed on a powder sample of mass $m=16$ mg in the temperature range $1.7<T<270$ K using a superconducting quantum interference device (SQUID) magnetometer. ac susceptibility measurements using a balanced-coil susceptometer were performed in the temperature range $0.125<T$

<8 K on single crystals of typical mass $m=20$ mg, in dc fields up to 9 T oriented parallel to the **c** axis. Specific-heat measurements were performed on a single crystal of mass $m=4$ mg for $0.125<T<2.5$ K in fields up to 9 T using relaxation calorimetry[29] with the field oriented parallel to the **a*** axis.

The sample used for inelastic neutron-scattering measurements consisted of three deuterated single crystals with a total mass of $m=3.32$ grams coaligned within $0.8°$. Measurements in the $(0kl)$ and $(h0l)$ scattering planes were performed on the SPINS cold neutron triple axis spectrometer at the National Institute of Standards and Technology (NIST) Center for Neutron Research in Gaithersburg, MD. The horizontal beam collimation before the sample was $50'/k_i$ ($Å^{-1}$)-$80'$ for the $(0kl)$ measurements, and $50'/k_i$ ($Å^{-1}$)-$76'$ for the $(h0l)$ measurements. A liquid-nitrogen-cooled BeO filter was placed after the sample, and data were collected at fixed final energy $E_f=3.7$ meV. A horizontally focusing pyrolytic graphite [PG(002)] analyzer with acceptance angles of $2.7°\times7.2°$ in the horizontal and vertical plane, respectively, was used to increase the count rate at the expense of broadening the instrumental wave-vector resolution perpendicular to the scattered neutron wave vector k_f. At energy transfer $\hbar\omega=0$, the energy resolution was $\delta\hbar\omega=0.13$ meV, and the instrumental resolution ellipsoid[30] projected on the scattering plane had full width at half maximum (FWHM) principal axes $\delta Q_1=0.043$ $Å^{-1}$ and $\delta Q_2=0.076$ $Å^{-1}$.

Measurements in the $(hk0)$ plane were performed on the BT2 thermal neutron triple axis spectrometer at NIST. Horizontal collimations of $60'-20'-20'-60'$ were used, and data were collected at $E_f=13.7$ meV with a PG filter before the analyzer. This gave typical FWHM resolutions at $\hbar\omega=0$ of $\delta\hbar\omega=0.84$ meV, and $\delta Q_\parallel=0.02$ $Å^{-1}$ and $\delta Q_\perp=0.09$ $Å^{-1}$ parallel and perpendicular to **Q**, respectively. All data were converted to the normalized scattering intensity $\tilde{I}(\mathbf{Q},\hbar\omega)$ following a procedure detailed elsewhere,[31] using the incoherent elastic scattering of the sample as measured in each experimental configuration.

IV. EXPERIMENTAL RESULTS

A. Magnetic susceptibility

The dc magnetic susceptibility $\chi(T)=M/H$ for a powder sample of PHCC is shown in Fig. 2. The data were taken in an applied field $H=50$ Oe, and the magnetization M was found to be linear in field up to $H=1$ T at $T=1.8$ K. As shown in the inset of Fig. 2, $\chi(T)$ rises with decreasing T to a rounded maximum at $T\approx12$ K, followed by a rapid decrease, as has been previously observed.[26,27] The low-temperature behavior of $\chi(T)$ is shown in the main panel of Fig. 2, which also includes single-crystal ac susceptibility data measured down to $T=0.125$ K. Apart from a paramagnetic background at the lowest temperatures that is attributable to residual impurities, these data show the exponentially activated dependence of $\chi(T)$ characteristic of a gapped Heisenberg antiferromagnet.
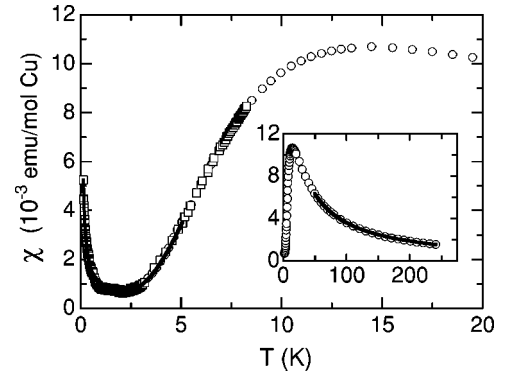

FIG. 2. Magnetic susceptibility $\chi(T)$ of PHCC. Open circles: dc suceptibility of powder. Open squares: ac susceptibility of single crystal. Inset: solid line is a fit to a Curie-Weiss law. Main frame: solid line is a fit to the asymptotic low-temperature susceptibility of a 2D gapped system as described in the text.

The ac magnetic susceptibility for a single crystal as a function of applied magnetic field at fixed temperature is shown in Fig. 3. The sharp feature in the data indicates an abrupt change in the magnetic density of states of PHCC as the spin gap closes at the critical field $H_{C1}\approx7.5$ T at $T=0.125$ K. This feature moves to larger magnetic field as the temperature is increased, and eventually becomes smeared out due to thermal population of multiple energy levels above the spin gap.

B. Specific heat

Figure 4 depicts the heat capacity as a function of temperature measured for different fixed magnetic fields up to $H=9$ T. The lattice contribution to the heat capacity has not been subtracted from the data. The exponentially activated heat capacity, which is apparent from the inset to Fig. 4 for fields $H<8$ T, is further direct evidence for a spin gap in PHCC. As H is increased, there is an increase in the specific heat at lower temperatures and the activation energy decreases, effects that indicate that the spin gap is decreasing.
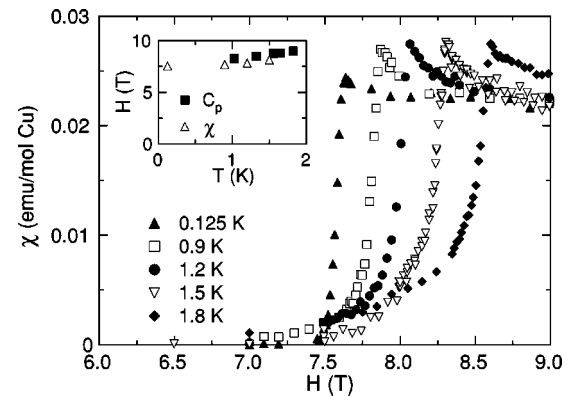

FIG. 3. ac magnetic susceptibility $\chi(H)$ of single-crystal PHCC at constant temperatures $T=0.125$, 0.9, 1.2, 1.5, and 1.8 K. Inset: Portion of H-T phase diagram of PHCC derived from specific-heat (filled squares) and magnetic-susceptibility (triangles) data.
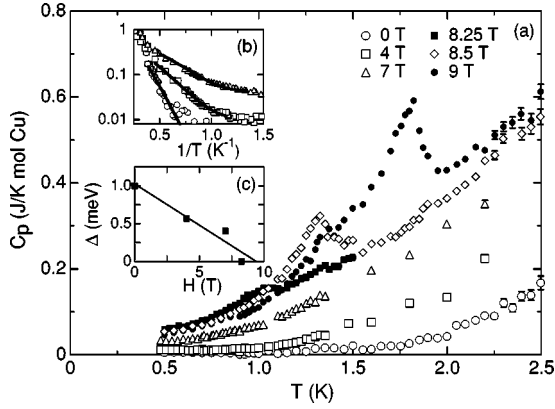
FIG. 4. Specific heat of PHCC versus temperature at constant applied magnetic field. (b) shows activated behavior at low fields and fits used to determine field-dependence of the spin gap shown in (c).

While at these lower fields no anomalous behavior in the temperature dependence of the specific heat is observed within the experimental uncertainty of our measurement, a peaklike singularity, indicative of of a phase transition, clearly appears at $H > 8$ T. This implies that above H_{C1} PHCC enters a 3D-ordered phase, as is typical of gapped quantum antiferromagnets.[21,31–34] Both the transition temperature and the the spin entropy removed from the system via the transition increase with H.

C. Inelastic neutron scattering

To map out the wave-vector dependence of the magnetic excitation spectrum of PHCC, energy transfer scans at constant **Q** were performed at 93 different locations throughout the reciprocal space of PHCC in zero magnetic field at $T = 1.5$ K. Figure 5 depicts the three reciprocal-lattice planes and the particular points in reciprocal space that were probed. At every wave vector measured, the spectrum is dominated by a single, resolution-limited mode. Representative energy scans are shown in Figs. 6–8. They illustrate dispersion of this mode along the h and l directions and the absence of dispersion as wave vector transfer varies along the k direction. The mode disappears upon heating to $T = 50$ K, as shown in Fig. 7(a), demonstrating that the observed scattering is magnetic in origin. The mode has its minimum energy (spin gap) $\Delta = 1$ meV at $\mathbf{Q} = (0.5, 0, 1.5)$ [Fig. 8(a)]. The full dispersion of this mode is summarized in Figs. 9–11. Each point in these figures was obtained by fitting a scan such as those in Figs. 6–8 to a Gaussian line shape. From these figures, the two-dimensional nature of the magnetic interactions of PHCC becomes clear. Figures 9(d) and 11(d) show significant dispersion along lines in reciprocal space that intersect the two-dimensional magnetic zone center at $\mathbf{Q} = (0.5, 0, 1.5)$, with somewhat stronger dispersion along h than along l. Along the edges of the magnetic zone, additional dispersion with h is seen in Figs. 9(a)–9(c), but only minimal variation in peak position was observed with l in Figs. 11(a)–11(c). From Fig. 10, an upper bound of 0.2(2) meV can be set on variation of the mode energy with k. The
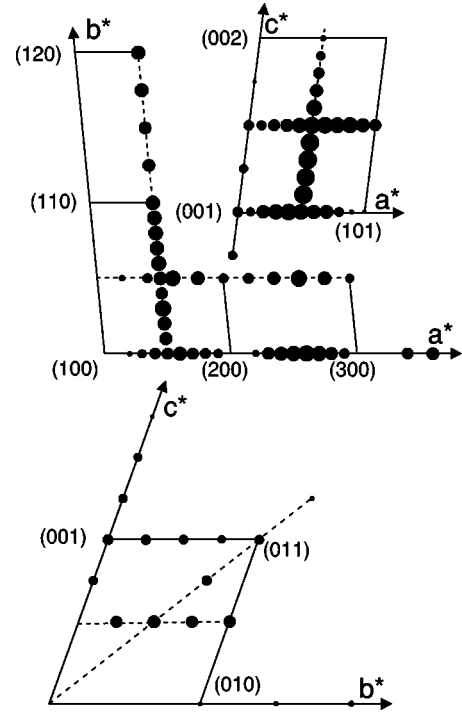

FIG. 5. Points in reciprocal space measured using inelastic neutron scattering. The area of each point is proportional to the measured first moment of the spectrum at that **Q**.

solid curves in Figs. 6–11 result from a fit using a two-dimensional model for the dynamic spin correlation function as described below.

V. DISCUSSION

A. Magnetic susceptibility

The zero-field susceptibility data yield significant information about the microscopic spin Hamiltonian. First, a mea-
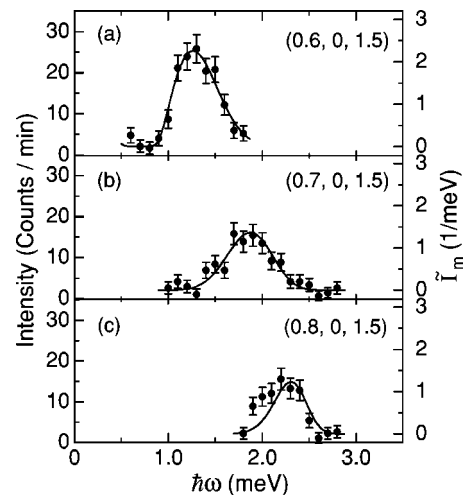

FIG. 6. Inelastic neutron scattering data for PHCC at $T = 1.5$ K showing dispersion of magnetic excitation with h. Right axis shows normalized magnetic scattering intensity $\tilde{I}_m(\mathbf{Q}, \omega)$. The solid lines are a fit to a two-dimensional model described in the text.
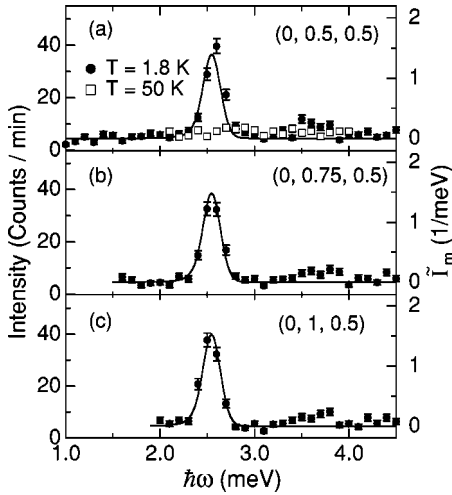
FIG. 7. Inelastic neutron-scattering data for PHCC at $T = 1.5$ K showing lack of dispersion of magnetic excitation with k. Open symbols in (a): data taken at $T = 50$ K. Right axis shows normalized magnetic scattering intensity $\tilde{I}_m(\mathbf{Q}, \omega)$. The solid lines are a fit to a two-dimensional model described in the text.

sure of the size of the spin gap may be obtained. In D dimensions, the asymptotic low-temperature susceptibility of a gapped spin system with quadratic dispersion[35] is proportional to

$$\chi(T) \propto T^{(D/2)-1} e^{-\Delta/k_B T}. \qquad (1)$$

The solid line in the main panel of Fig. 2 is a fit to the two-dimensional form of Eq. (1), including a diamagnetic background and a low-temperature Curie tail. The fit was restricted to $T \lesssim 5$ K, and gave a spin gap $\Delta = 1.2(1)$ meV, in good agreement with that observed in the neutron-scattering data.
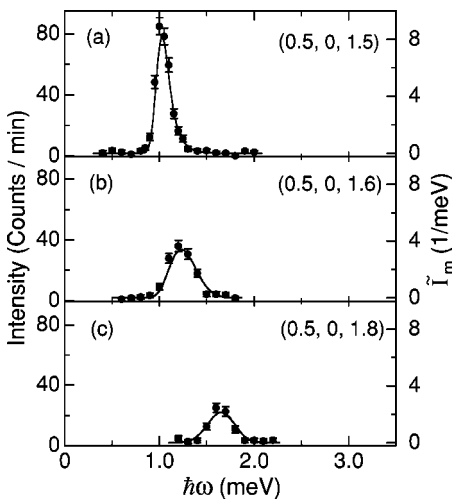

FIG. 8. Inelastic neutron-scattering data for PHCC at $T = 1.5$ K showing dispersion of magnetic excitation with l. Right axis shows normalized magnetic scattering intensity $\tilde{I}_m(\mathbf{Q}, \omega)$. The solid lines are a fit to a two-dimensional model described in the text.
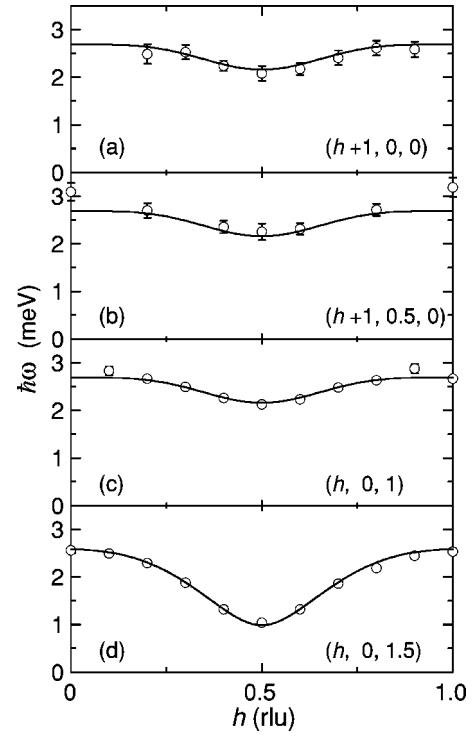

FIG. 9. Energy of magnetic excitations in PHCC showing dispersion with h at constant k and l. Data points are determined from Gaussian fits to constant-$\mathbf{Q}$ scans. The solid lines are a fit to a two-dimensional model described in the text.

FIG. 10. Energy of magnetic excitations in PHCC showing lack of dispersion with k at constant h and l. Data points are determined from Gaussian fits to constant-$\mathbf{Q}$ scans. The solid lines are fit to a two-dimensional model described in the text.
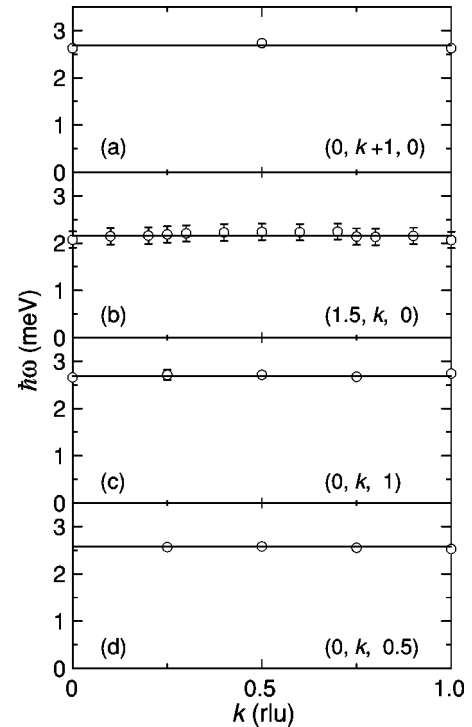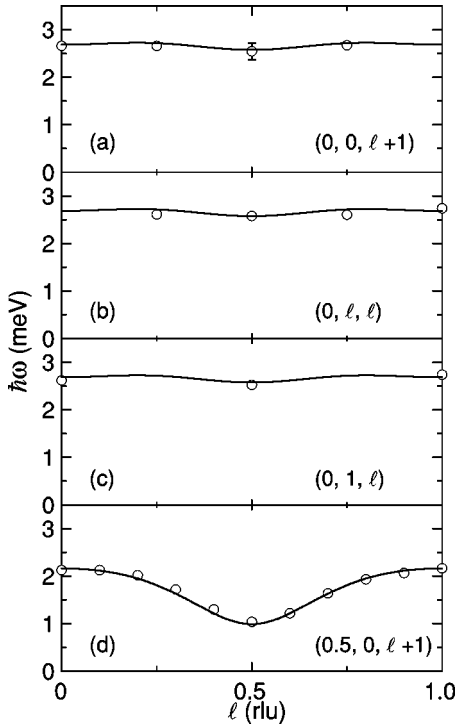
FIG. 11. Energy of magnetic excitations in PHCC showing dispersion with l. Data points are determined from Gaussian fits to constant-**Q** scans. The solid lines are fit to a two-dimensional model described in the text.

From the high-temperature Curie-Weiss behavior of $\chi(T)$ we obtain a value for the sum of all relevant exchange constants in the system,

$$J_0 = \sum_{\mathbf{d}} J_{\mathbf{d}}, \tag{2}$$

where $\{\mathbf{d}\}$ is the set of bonds connecting a spin to its neighbors. Fitting the sum of a diamagnetic and a Curie-Weiss term to our $\chi(T)$ data in the temperature range $50 < T < 250$ K we extracted the Curie-Weiss temperature Θ_{CW}, the average g factor, and the diamagnetic term resulting from the sample and sample holder. The fit is shown as a solid line in the inset to Fig. 2. The Curie-Weiss temperature $\Theta_{CW} = -19.0(7)$ K is related to J_0 through $\Theta_{CW} = S(S+1)J_0/3k_B$.[36] Solving for the sum of the independent exchange constants, we find $J_0 = 3.3(1)$ meV while $g_{av} = 2.2(3)$. A similar estimate for J_0 is obtained by fitting $\chi(T)$ to an alternating spin chain model.[26,27] This reflects the insensitivity of the zero-field susceptibility to the geometry of the magnetic interactions.

B. Specific heat

The change in the activated temperature dependence of the specific heat with increasing magnetic field for $H < 8$ T gives a measure of the reduction of the spin gap as the lower critical field is approached. The asymptotic low-temperature form for the specific heat, derived under the same conditions as for Eq. (1), is given by

$$C_p(T) \propto T^{(D/2)-2} e^{-\Delta/k_B T}. \tag{3}$$

The solid lines in Fig. 4(b) are fits to this form for $D = 2$, with the addition of a term proportional to H^2/T^2 to account for nuclear spin contributions at the lowest temperatures. The derived gap values are shown versus the applied field in Fig. 4(c). The approximately linear reduction of the spin gap with field is consistent with the Zeeman splitting of a triplet of excited states.

The positions of the peaks observed in the temperature dependent specific heat for $H > 8$ T outline the lower edge of the ordered region of the H-T phase diagram. This phase boundary is shown in the inset to Fig. 3. Clearly, further work is required to map out the full extent of the ordered phase and also to determine the structure and symmetry of the order parameter. The locations of peaks in the field-dependent, single-crystal magnetic susceptibility data are also shown in the inset to Fig. 3. Taking into account the anisotropic g tensor of PHCC,[27] these data are entirely consistent with the specific-heat data.

C. Inelastic neutron scattering

The magnetic contribution $\tilde{I}_m(\mathbf{Q}, \hbar\omega)$ to the normalized neutron-scattering intensity $\tilde{I}(\mathbf{Q}, \hbar\omega)$ is related to the dynamic spin-correlation function $\mathcal{S}^{\alpha\beta}(\mathbf{Q}, \omega)$ as follows:[31,37]

$$\tilde{I}_m(\mathbf{Q}, \hbar\omega) = \int d^3Q' \hbar d\omega' \mathcal{R}_{\mathbf{Q},\omega}(\mathbf{Q} - \mathbf{Q}', \omega - \omega')$$

$$\times \left| \frac{g}{2} F(Q') \right|^2 \sum_{\alpha\beta} (\delta_{\alpha\beta} - \hat{Q}'_\alpha \hat{Q}'_\beta) \mathcal{S}^{\alpha\beta}(\mathbf{Q}', \omega'). \tag{4}$$

Here $F(Q)$ is the magnetic form factor of the Cu^{2+} ion and $\mathcal{R}_{\mathbf{Q}\omega}$ is the normalized instrumental resolution function.[30] We assume that the magnetic Hamiltonian is isotropic in spin space, and thus since no symmetry-breaking ordering transition occurs in PHCC at zero field, the dynamic spin-correlation function should also be isotropic. This is supported by previous susceptibility measurements, which indicate that exchange anisotropy in PHCC is very small,[27] and by the absence of any observable anisotropy splitting of the excitations observed by neutron scattering. In this case the different spin polarizations in Eq. (4) can be summed to give

$$\sum_{\alpha\beta} (\delta_{\alpha\beta} - \hat{Q}'_\alpha \hat{Q}'_\beta) \mathcal{S}^{\alpha\beta}(\mathbf{Q}', \omega') = 2\mathcal{S}^{\alpha\alpha}(\mathbf{Q}', \omega'). \tag{5}$$

Owing to the low symmetry of PHCC, there are a large number of potential Cu-Cu magnetic interactions within the **a-c** plane. Information about the relative importance of spin pair correlations to the ground-state energy can be obtained in a model-independent way through the first moment sum rule.[38] For an isotropic spin system, this is
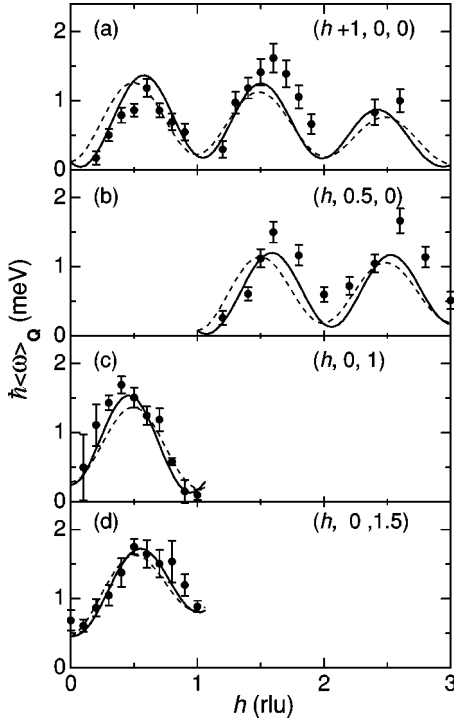
FIG. 12. Variation of first moment $\hbar\langle\omega\rangle_{\mathbf{Q}}$ of PHCC with h at constant k and l. Data points are determined by fitting each original constant-$\mathbf{Q}$ scan to a Gaussian peak and calculating the first moment of the intensity from that fit. The dashed (solid) lines are determined by a global fit including six(eight) Cu-Cu interactions, as described in the text.

FIG. 13. Variation of first moment $\hbar\langle\omega\rangle_{\mathbf{Q}}$ of PHCC with k at constant h and l. Data points are determined by fitting each original constant-$\mathbf{Q}$ scan to a Gaussian peak and calculating the first moment of the intensity from that fit. The dashed (solid) lines are determined by a global fit including six(eight) Cu-Cu interactions, as described in the text.

$$\hbar\langle\omega\rangle_{\mathbf{Q}}\equiv\hbar^2\int_{-\infty}^{\infty}\omega\mathcal{S}^{\alpha\alpha}(\mathbf{Q},\omega)d\omega$$

$$=-\frac{1}{3}\sum_{\mathbf{d}}J_{\mathbf{d}}\langle\mathbf{S}_0\cdot\mathbf{S}_{\mathbf{d}}\rangle(1-\cos\mathbf{Q}\cdot\mathbf{d}),\qquad(6)$$

where $J_{\mathbf{d}}$ is the exchange strength and $\langle\mathbf{S}_0\cdot\mathbf{S}_{\mathbf{d}}\rangle$ is the two-spin-correlation function for the spin-pair with bond vector $\mathbf{d}$. We write the Hamiltonian in the form

$$\mathcal{H}=\frac{1}{2}\sum_{\mathbf{r},\mathbf{d}}J_{\mathbf{d}}\mathbf{S}_{\mathbf{r}}\cdot\mathbf{S}_{\mathbf{r}+\mathbf{d}},\qquad(7)$$

where the index $\{\mathbf{r}\}$ runs over all spins. The ground-state energy per spin E_0 is closely related to the first moment, being simply

$$E_0=\frac{1}{2}\sum_{\mathbf{d}}J_{\mathbf{d}}\langle\mathbf{S}_0\cdot\mathbf{S}_{\mathbf{d}}\rangle.\qquad(8)$$

The first frequency moment of the dynamic correlation function $\hbar\langle\omega\rangle_{\mathbf{Q}}$ measured in PHCC is shown in Fig. 5 and Figs. 12–14. The data points were obtained from the same Gaussian fits that were used to determine the mode energy.

Unlike what is observed in strongly dimerized spin-gap systems, the variation of $\hbar\langle\omega\rangle_{\mathbf{Q}}$ with $\mathbf{Q}$ in PHCC cannot be accounted for by a single spin pair. Instead, several crystallographically distinct spin pairs are strongly correlated and
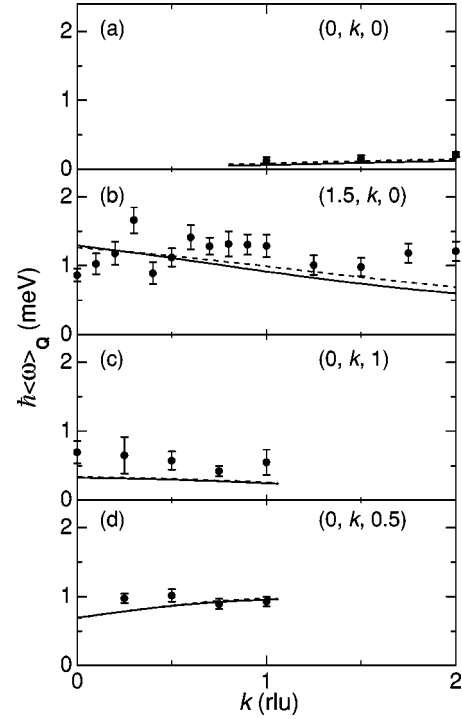
contribute significantly to the ground-state energy. This renders the system considerably more intricate to describe theoretically. For example, the RPA theory based on a dimerized ground state that accounts for strongly dimerized systems in one, two, and three dimensions[4,5,18,20,23] is not adequate here since a single spin pair controls the first moment of $\mathcal{S}^{\alpha\alpha}(\mathbf{Q},\omega)$ in that model.

In the absence of an adequate theory of gapped spin systems for $D>1$ that goes beyond a dimer-based expansion, we parametrize the measured dispersion $E(\mathbf{Q})$ in PHCC with the following phenomenological expression, consistent with Bloch's theorem:

$$E(\mathbf{Q})=(B_0+B_h\cos(2\pi h)+B_l\cos(2\pi l)$$
$$+B_{hl}\{\cos[2\pi(h+l)]+\cos[2\pi(h-l)]\}$$
$$+B_{2h}\cos(4\pi h)+B_{2l}\cos(4\pi l))^{1/2}.\qquad(9)$$

We note that simpler dispersion relations of the form $E(\mathbf{Q})=A_0+\Sigma_i A_i\cos(\mathbf{Q}\cdot\mathbf{R}_i)$, which provide an effective description of related systems with weaker dispersion such as CuHpCl,[42] do not provide a good description of the dispersion in PHCC. Because most of the observed magnetic intensity comes in the form of resolution-limited peaks, we can use the single mode approximation (SMA) for the dynamic correlation function,

$$\mathcal{S}^{\alpha\alpha}(\mathbf{Q},\omega)=\mathcal{S}(\mathbf{Q})\delta(\hbar\omega-E(\mathbf{Q})),\qquad(10)$$
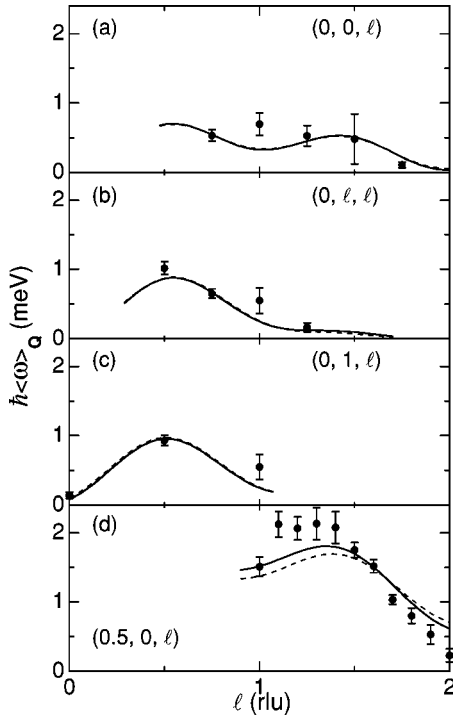
FIG. 14. Variation of first moment $\hbar\langle\omega\rangle_{\mathbf{Q}}$ of PHCC with l. Data points are determined by fitting each original constant-$\mathbf{Q}$ scan to a Gaussian peak and calculating the first moment of the intensity from that fit. The dashed (solid) lines are determined by a global fit including six(eight) Cu-Cu interactions, as described in the text.

for quantitative analysis of the data. Here $\mathcal{S}(\mathbf{Q})$ is the static structure factor, which is the Fourier transform of the equal-time two-spin-correlation function, and quantifies the energy-integrated intensity [it is the zeroth moment of $\mathcal{S}^{\alpha\alpha}(\mathbf{Q},\omega)$]. The polarization index α may be omitted for an isotropic spectrum. The SMA has been used successfully for gapped spin chains,[5,39] and other quantum many-body systems[40] where a single, coherent mode dominates the excitation spectrum. Using the SMA expression [Eq. (10)] in the first moment sum rule [Eq. (6)] one can establish a relation between the measured intensities and the dispersion relation $E(Q)$,

$$\mathcal{S}(\mathbf{Q}) = -\frac{1}{3E(\mathbf{Q})} \sum_{\mathbf{d}} J_{\mathbf{d}}\langle\mathbf{S}_0\cdot\mathbf{S}_{\mathbf{d}}\rangle(1-\cos\mathbf{Q}\cdot\mathbf{d}), \quad (11)$$

that involves the spin-pair correlations which contribute to the ground-state energy.

We have carried out global fits to $\tilde{I}_m(\mathbf{Q},\hbar\omega)$ for our entire data set, using Eqs. (9)–(11) as input to Eq. (4). For each energy scan, the nonmagnetic background was modeled by a constant plus a Gaussian peak centered at $\hbar\omega=0$ to account for incoherent elastic scattering as needed. To determine the simplest parametrization of the data, global fits were carried out with varying numbers of terms included in Eq. (11). The results of these fits with bonds 1–6 and bonds 1–8 in Fig. 1 are given in Tables I and II. Further neighbor bonds gave no measurable contribution when included in the fits. Examples of the line shapes derived from the eight-bond fit are shown

TABLE II. Fitted parameters in the dispersion relation, Eq. (9), for the six- and eight-bond fits of the PHCC inelastic neutron-scattering data.

Parameter	6 bonds (meV^2)	8 bonds (meV^2)
B_0	5.44(2)	5.45(2)
B_h	2.06(3)	2.05(3)
B_l	1.07(3)	1.06(3)
B_{hl}	−0.39(1)	−0.39(1)
B_{2h}	−0.34(3)	−0.35(3)
B_{2l}	−0.22(2)	−0.23(2)

as solid lines in Figs. 6–8. The right-hand vertical scale in these figures gives the normalized magnetic intensity $\tilde{I}_m(\mathbf{Q},\hbar\omega)$. Magnetic neutron scattering from a local moment magnet satisfies a total moment sum rule that can be expressed as

$$\langle S^2 \rangle = \frac{\hbar\int d^3Q\,d\omega\sum_{\alpha\beta}\mathcal{S}^{\alpha\beta}(\mathbf{Q},\omega)}{\int d^3Q} = S(S+1). \quad (12)$$

Clearly we do not have enough data to carry out the complete integration. However, we can ask whether the SMA, which accounts for the scattering data where available, satisfies the sum rule. Carrying out the $\mathbf{Q}$ integration of Eq. (11) numerically, we obtain $\langle S^2\rangle=0.8(2)$. The result being indistinguishable from $S(S+1)=3/4$ suggests that the resonant mode accounted for by the SMA carries most of the spectral weight in PHCC.

The dispersion relation determined from the eight-bond global fit is shown as solid lines in Figs. 9–11. It is consistent with the data derived directly from the raw data, indicating that the variational dispersion relation Eq. (9) used in the SMA is general enough not to cause significant bias. As may be seen from Table II, the parameters in Eq. (9) are well determined, and the results for the six- and eight-bond fits are indistinguishable.

The first moment calculated from the model with the parameters determined from the global fits is shown in Figs. 12–14 as dashed and solid lines for the six-bond and eight-bond fits, respectively. Instrumental resolution effects were included in this calculation. The agreement with the first moment determined from the Gaussian fits to individual scans is in general quite good, with modest improvement in the quality of the eight-bond fit over the six-bond fit. There is also good quantitative agreement for the terms common to both fits, particularly for the larger terms, indicating the robustness of the numbers determined through this analysis.

Without a microscopic model that connects exchange constants with the dispersion relation, it is not possible to determine $J_{\mathbf{d}}$ and $\langle\mathbf{S}_0\cdot\mathbf{S}_{\mathbf{d}}\rangle$ independently. Instead one measures their products, which determine the contribution of each bond to the ground-state energy E_0 [Eq. (8)]. In fact, because $|\langle\mathbf{S}_0\cdot\mathbf{S}_{\mathbf{d}}\rangle|<3/4$, each term provides a lower bound on the

magnitude of the corresponding exchange interaction. In Fig. 1(c), the thickness of the Cu-Cu bonds is proportional to $|J_{\mathbf{d}}\langle \mathbf{S}_0 \cdot \mathbf{S}_{\mathbf{d}}\rangle|$. From this figure and from Table I, we see that the largest Cu-Cu interaction is bond 1, the "dimer" predicted previously.[27] However, other bonds also show significant antiferromagnetic correlations, particularly bonds 3 and 6. These bonds are noteworthy as they provide uniform, albeit anisotropic, linkage of a macroscopic two-dimensional spin system. It is also important to note that several bonds give a positive contribution to the first moment. These bonds, shown as gray lines in Fig. 1(c), are frustrated by definition as they raise the ground-state energy.

Summing up all terms shown in Table I we find the ground-state energy per spin $E_0 = -1.5(4)$ meV for both the six- and eight-bond fits. Using the measured value of spin gap $\Delta = 1$ meV, we can thus determine the relation $E_0 \approx -1.5 \cdot \Delta$, which can be used to quantify explicitly the correspondence of the spin system of PHCC to a particular quantum-disordered 2D spin model. It also helps to position PHCC on the phase diagram of the 2D QHAFM,[8] characterizing how close it is to quantum criticality.

VI. CONCLUSIONS

The set of measurements presented here establish PHCC as a clean example of a two-dimensional spin-singlet system with a gap. The susceptibility and heat-capacity data show evidence of a quantum phase transition from the gapped phase to a Néel-ordered state at a magnetic field $H_{c1} \approx 7.5$ T. This transition appears qualitatively similar to that observed in many other spin-gap systems.[21,31–34] However, the coupled-dimer picture that describes previously studied 2D and 3D spin gap materials is not appropriate for PHCC. This material lies in an unusual region of the phase space of the model, in a quantum disordered regime close to the quantum-critical point. Although we are not yet able to associate unambiguously the zero-field ground state with either a

particular kind of valence bond crystal or a RVB-type spin liquid, it is clear that frustration plays a key role in defining it. It is worth noting that evidence for spin-frustration effects was recently observed in CuHpCl,[42] another quasi-2D spin system, as well as in $SrCu_2(BO_3)_2$,[24] and thus it may be that frustration is in fact a common feature of low-symmetry, gapped spin systems.

Another issue that becomes increasingly important as one moves towards the QC point, or from the dimerized limit toward a system with more uniform coupling, is the appearance of a continuum in the spin-fluctuation spectrum. In the quantum-disordered 2D HAFM models this is described in terms of spinon deconfinement,[41] while in the strongly dimerized limit it is usually adequately accounted for by multimagnon excitations. There are some features in the present data indicating that a continuum may be detectable in PHCC (e.g., the broad, weak feature at $\hbar\omega \approx 3.5$ meV in Fig. 7), but further experiments are required to clarify this issue. Finally, the low-energy scales in PHCC make it an excellent candidate for further studies of quantum critical and field-dependent phenomena in a two-dimensional gapped spin system with frustration.

[1] C. Broholm, D. H. Reich, G. Aeppli, S.-H. Lee, D. C. Dender, P. R. Hammar, G. Xu, J. F. DiTusa, and A. P. Ramirez, in *Dynamical Properties of Unconventional Magnetic Systems*, edited by A. T. Skjeltorp and D. Sherrington (Kluwer, Dordrecht, 1998), p. 77.

[2] S. A. Carter, B. Batlogg, R. J. Cava, J. J. Krajewski, W. F. Peck, Jr., and T. M. Rice, Phys. Rev. Lett. **77**, 1378 (1996).

[3] R. S. Eccleston, M. Uehara, J. Akimitsu, H. Eisaki, N. Motoyama, and S. Uchida, Phys. Rev. Lett. **81**, 1702 (1998).

[4] M. Matsuda, T. Yoshihama, K. Kakurai, and G. Shirane, Phys. Rev. B **59**, 1060 (1999).

[5] G. Xu, C. Broholm, D. H. Reich, and M. A. Adams, Phys. Rev. Lett. **84**, 4465 (2000).

[6] A. W. Garrett, S. E. Nagler, T. Barnes, and B. C. Sales, Phys. Rev. B **55**, 3631 (1997).

[7] A. W. Garrett, S. E. Nagler, D. A. Tennant, B. C. Sales, and T. Barnes, Phys. Rev. Lett. **79**, 745 (1997).

[8] S. Chakravarty, B. I. Halperin, and D. R. Nelson, Phys. Rev. Lett.

60, 1057 (1988); Phys. Rev. B **39**, 2344 (1989).

[9] S. Sachdev, *Quantum Phase Transitions* (Cambridge University Press, New York, 2000).

[10] R. R. P. Singh, M. P. Gelfand, and D. A. Huse, Phys. Rev. Lett. **61**, 2484 (1988).

[11] K. Ueda, Phys. Rev. Lett. **76**, 3822 (1996).

[12] M. E. Zhitomirsky and K. Ueda, Phys. Rev. B **54**, 9007 (1996).

[13] S. Sachdev, Phys. Rev. B **45**, 12 377 (1992).

[14] R. R. P. Singh and D. A. Huse, Phys. Rev. Lett. **68**, 1766 (1992).

[15] M. Mambrini and F. Mila, Eur. Phys. J. B **17**, 651 (2000).

[16] S. Liang, B. Doucot, and P. W. Anderson, Phys. Rev. Lett. **61**, 365 (1988).

[17] R. Moessner and S. L. Sondhi, Phys. Rev. Lett. **86**, 1881 (2001).

[18] B. Leuenberger, A. Stebler, H. U. Güdel, A. Furrer, R. Feile, and J. K. Kjems, Phys. Rev. B **30**, 6300 (1984).

[19] T. Kato, K. Takatsu, H. Tanaka, W. Shiramura, M. Mori, K. Nakajima, and K. Kakurai, J. Phys. Soc. Jpn. **77**, 752 (1998).

[20] N. Cavadini, W. Henggeler, A. Furrer, H. U. Güdel, K. Krämer,

and H. Mutka, Eur. Phys. J. B **7**, 519 (1999).

[21] A. Oosawa, M. Ishii, and H. Tanaka, J. Phys.: Condens. Matter **11**, 265 (1999); A. Oosawa, A. Katori, and H. Tanaka, Phys. Rev. B **63**, 134416 (2001).

[22] N. Cavadini, G. Heigold, W. Henggler, A. Furrer, H.-U. Güdel, K. Krämer, and H. Mutka, Phys. Rev. B **63**, 172414 (2001).

[23] Y. Sasago, K. Uchinokura, A. Zheludev, and G. Shirane, Phys. Rev. B **55**, 8357 (1997).

[24] H. Kageyama, K. Yoshimura, R. Stern, N. V. Mushnikov, K. Onizuka, M. Kato, K. Kosuge, C. P. Slichter, T. Goto, and Y. Ueda, Phys. Rev. Lett. **82**, 3168 (1999).

[25] H. Kageyama, M. Nishi, N. Aso, K. Onizuka, T. Yosihama, K. Nukui, K. Kodama, K. Kakurai, and Y. Ueda, Phys. Rev. Lett. **84**, 5876 (2000).

[26] L. P. Battaglia, A. B. Corradi, U. Geiser, R. Willett, A. Motori, F. Sandrolini, L. Antolini, T. Manfredini, L. Menabue, and G. C. Pellacani, J. Chem. Soc. Dalton Trans. **2**, 265 (1988).

[27] A. Daoud, A. Ben Salah, C. Chappert, J. P. Renard, A. Cheikhrouhou, T. Duc, and M. Verdaguer, Phys. Rev. B **33**, 6253 (1986).

[28] L. P. Regnault, J. Rossat-Mignod, J. P. Renard, M. Verdaguer, and C. Vettier, Physica B **156-157**, 247 (1989).

[29] B. Bachmann, F. J. DiSalvo, Jr., T. H. Geballe, R. L. Greene, R. E. Howard, C. N. King, H. C. Kirsch, K. N. Lee, R. E. Schwall, H.-U. Thomas, and R. B. Zubeck, Rev. Sci. Instrum. **43**, 205 (1972).

[30] N. D. Chesser and J. D. Axe, Acta Crystallogr., Sect. A: Cryst.

Phys., Diffr., Theor. Gen. Crystallogr. **A29**, 160 (1973).

[31] P. R. Hammar, D. H. Reich, C. Broholm, and F. Trouw, Phys. Rev. B **57**, 7846 (1998).

[32] K. M. Diederix, H. A. Algra, J. P. Groen, T. O. Klassen, N. J. Poulis, and R. L. Carlin, Phys. Lett. **60A**, 247 (1977).

[33] J. Eckert, D. E. Cox, G. Shirane, S. A. Friedberg, and H. Kobayashi, Phys. Rev. B **20**, 4596 (1979).

[34] Z. Honda, H. Asakawa, and K. Katsumata, Phys. Rev. Lett. **81**, 2566 (1998).

[35] M. Troyer, H. Tsunetsugu, and D. Würtz, Phys. Rev. B **50**, 13 515 (1994).

[36] N. W. Ashcroft and N. D. Mermin, *Solid State Physics* (Saunders College Publishing, Fort Worth, TX, 1976).

[37] We use the notation of S. W. Lovesey, *Theory of Neutron Scattering from Condensed Matter* (Clarendon Press, Oxford, 1984).

[38] P. C. Hohenberg and W. F. Brinkman, Phys. Rev. B **10**, 128 (1974).

[39] S. Ma, C. Broholm, D. H. Reich, B. J. Sternlieb, and R. W. Erwin, Phys. Rev. Lett. **69**, 3571 (1992).

[40] S. M. Girvin, A. H. MacDonald, and P. M. Platzman, Phys. Rev. B **33**, 2481 (1986).

[41] A. V. Chubukov and O. A. Starykh, Phys. Rev. B **52**, 440 (1995).

[42] M. B. Stone, J. Rittner, Y. Chen, H. Yardimici, D. H. Reich, C. Broholm, D. V. Ferraris, and T. Lectka, cond-mat/0103023 (unpublished).